energy&fuels

Article

Cite This: Energy Fuels 2018, 32, 314−328

pubs.acs.org/EF

Advances in Asphaltene Petroleomics. Part 2: Selective Separation Method That Reveals Fractions Enriched in Island and Archipelago Structural Motifs by Mass Spectrometry

Martha L. Chacón-Patiño,[†] Steven M. Rowland,[*,†,‡] and Ryan P. Rodgers[*,†,‡,§]

[†]National High Magnetic Field Laboratory and [‡]Future Fuels Institute, Florida State University, 1800 East Paul Dirac Drive, Tallahassee, Florida 32310, United States

[§]Department of Chemistry and Biochemistry, Florida State University, 95 Chieftain Way, Tallahassee, Florida 32306, United States

Supporting Information

ABSTRACT: Advances in high-resolution Fourier transform ion cyclotron resonance mass spectrometry (FT-ICR MS) enable molecular-level characterization of ultracomplex asphaltene samples. Such analyses most often reveal compounds that are highly aromatic but alkyl-deficient in nature and, thus, support the classical "island" model of asphaltene architecture. However, recent works that combine chromatographic separations with mass spectrometry for the analysis of crude oils have shown that differences in ionization may greatly affect the analysis of complex mixtures (known as the matrix effect). Simply, compounds that ionize with greater efficiency are preferentially observed and mask the detection of poorly ionized compounds. Asphaltenes are not immune to this phenomenon. In the first of this series (10.1021/acs.energyfuels.7b02873), it was demonstrated that asphaltenes generated by different precipitants showed greatly varied monomer ion yields (ionization efficiencies). This work focuses on the development of an extrography fractionation method that selectively targets the removal of asphaltene species that exhibit high monomer ion yields and, thus, restrict mass spectral characterization of less efficiently ionized species. Silica gel was used as the stationary phase, and a unique solvent series separated asphaltenes based on their interaction with the silica surface, which was later determined to depend heavily upon the structure as well as monomer ion yield. The first two solvents (acetone and acetonitrile) isolated compounds that most efficiently produce monomeric asphaltene ions and, thus, cause bias in mass spectrometric analyses of whole asphaltenes. A solvent polarity gradient was then used, with *n*-heptane, toluene, tetrahydrofuran, and methanol, to separate remnant asphaltene compounds on the basis of polarity and structure. Our results demonstrate that mass spectrometry of whole asphaltenes does not reveal the complete molecular composition but rather preferentially exposes highly aromatic, alkyl-deficient, island-type structures. Early eluting fractions are shown to resemble the composition of the whole asphaltene and are enriched in island structures, whereas the analysis of later-eluting fractions reveals archipelago structural motifs as well as species with atypical asphaltene molecular compositions. We also demonstrate that, as molecular weight increases, the asphaltenes exhibit increased contributions of archipelago structural motifs. Higher mass ions (m/z > 550), even from asphaltene fractions enriched in island structures, exhibit fragmentation pathways that originate from archipelago structures. Thus, positive-ion atmospheric pressure photoionization (APPI) FT-ICR MS provides molecular-level data that suggest that the island model is not the dominant structure of asphaltenes. It coexists with abundant archipelago structures, and the ratios of each are sample-dependent.

INTRODUCTION

Asphaltenes are perhaps the most intriguing, complex, and polydisperse mixtures in analytical chemistry.[1−4] These enigmatic species are best known for their tendency to clog wells and pipelines,[5,6] trigger reservoir impairment,[7] stabilize emulsions,[8] and foul refinery equipment.[9] Understanding the molecular structure is of paramount importance to optimize the production and transport of asphaltene-rich oils and to maximize the yield of high-value products in refinery processes. However, abundant controversy about the characterization of these materials (chemistry and structure) has limited the development of robust methods to help prevent and ultimately solve asphaltene-related problems.[10−13]

To many in the field of petroleum chemistry, the term asphaltenes evokes a mental picture of a structure based on the island model.[14] This widely accepted and suported model suggests that most petroleum asphaltenes contain a fundamental, dominant structure, which consists of a single aromatic core of ∼7−15 fused rings with alkyl side chains.[15] Several reports suggest that the island model is well-supported by direct molecular imaging,[16] fluorescence depolarization,[17] and unimolecular fragmentations in mass spectrometry (MS).[18] However, this model is not consistent with the nature of the upgrading products from petroleum asphaltenes.[19,20] Most importantly, the island model fails to explain the presence of abundant benzene, naphthalene, and anthracene derivatives from thermally modified asphaltenes.[11,19,21−24] Thus, these observations gave rise to the archipelago model, which proposed that several aromatic cores are linked by alkyl or cycloalkyl bridges.[25,26] This model has received significant

Received: October 25, 2017
Revised: December 6, 2017
Published: December 7, 2017

DOI: 10.1021/acs.energyfuels.7b03281
Energy Fuels 2018, 32, 314−328

criticism, and several publications point out that it lacks the support of MS.[12,27] However, it is important to underscore the importance of the ionization process in mass spectral analyses. Simply put, the mass spectrometer detects ions. Whatever ions are generated by the source are available for detection by the mass spectrometer. Thus, it is imperative to highlight that complex mixtures, such as asphaltenes, require special attention as a result of differences in ionization efficiency between chemical species and, in the case of asphaltenes, their aggregation state.[2,28] Even with atmospheric pressure photoionization (APPI), thought to be the most suitable atmospheric ionization technique for asphaltenes,[28−30] the most easily ionized compounds are preferentially detected and often do not reflect the bulk elemental composition of the whole sample.[1,28,31] In APPI, molecules are converted to the gas phase prior to ionization through heated nebulization. Therefore, the ionization of monomer ions is dependent upon both ionization potential as well as their aggregation state prior to and during the ionization process. We previously reported that asphaltene samples subjected to extended cleaning processes with *n*-heptane ionize less efficiently in APPI compared to unclean asphaltenes, whereas maltene fractions exhibit 50-fold monomer ion yield when compared to "purified" asphaltene samples.[32]

MS Analysis of Whole Asphaltenes Is Incomplete. Recent reports on asphaltene characterization suggest that nanoaggregation restricts the complete characterization of asphaltenes by MS.[26,28,33] The concentrations required for MS analysis typically range between ∼100 and 300 ppm, whereas the critical nanoaggregation concentration for asphaltenes is ∼50 ppm.[28,34,35] Thus, only those compounds that exist in a non-aggregated state (monomers) are analyzed in the typical mass range of most commercial mass spectrometers ($200 < m/z < 2000$), although nanoaggregates can be detected with high-mass-range time-of-flight instruments.[34] McKenna et al.[28] demonstrated that asphaltene compositions observed by APPI−high-resolution MS exhibit H/C ratios lower than the bulk values. The preferential ionization of aromatics by APPI and the suspected, selective removal of higher H/C ratio asphaltenes through nanoaggregation are believed to be the causes of the discrepancies.[28,34] Hence, sample polydispersity and potential nanoaggregation are asphaltene characteristics that pose analytical challenges in MS analysis.

In 2008, Pomerantz et al.[36] reported an effort to overcome the limitations in analysis of asphaltenes by MS. They used two-step laser mass spectrometry (L^2MS) to purportedly produce purely monomeric and, thus, accurate molecular weight distributions from asphaltene samples. In this technique, the laser desorption and laser ionization steps are spatially and temporally separated, which according to the authors, prevents asphaltene aggregation.[37,38] However, it is important to point out that L^2MS is not suitable for the intact desorption/ionization of archipelago structures, because Pomerantz et al.[39] reported low survival yields for the molecular ions from archipelago model compounds. Thus, the fragmentation of archipelago compounds during ionization imparts a known compositional bias in the technique and is, therefore, not well suited to detect archipelago structural motifs.

Separations Are Essential in Petroleomics. Fractionation is a common way to address selective ionization (matrix effect) in MS analyses.[26,40−43] Separations designed for petroleum analyses commonly focus on the isolation of compound classes based on chemical functionality. Such separations have recently been applied to naphthenic acids, sulfides, and basic nitrogen.[44−49] However, even within these compound classes, there are large differences in ionization efficiency that have been well-documented for naphthenic acid, interfacially active, and basic nitrogen compounds.[41,47,50−52] The separations showed that low-molecular-weight compounds were preferentially ionized during positive- and negative-ion electrospray ionization (ESI) and that fractionation by hydrophobicity provided greater insight (up to 10-fold higher) into compounds not previously detected in direct analyses. Although APPI is thought of as a more uniform ionization technique compared to ESI, it would be short-sighted to assume that similar problems would not be possible for samples as complex as asphaltenes.

Not a New Idea but Crucial for MS Analysis. Previous efforts for asphaltene fractionation can be grouped into differential solubility and sequential adsorption−desorption from polar/nonpolar surfaces.[53−58] For instance, Buenrostro-González et al.[59] fractionated Maya asphaltenes by reprecipitation from toluene (Tol) solutions, with acetone and *n*-heptane as precipitating solvents. The authors reported that acetone-precipitated fractions have larger structural differences when compared to those obtained with *n*-heptane. Bulk elemental composition, nuclear magnetic resonance (NMR), and infrared spectroscopy indicated that the asphaltene fraction with the highest solubility in acetone concentrated the total content of vanadyl porphyrins and exhibited one of the highest aromaticity factors, with the lowest content of alkyl side chains. Additional studies by size-exclusion chromatography indicated that this fraction exhibits the longest retention times, which suggests a low propencity to aggregation.[59] In other reports, Boduszynski et al.,[53] Boysen and Schabron,[58] and Rogel et al.[60] reported on-column fractionation of asphaltenes based on solubility behavior. In this method, the sample is deposited on polytetrafluoroethylene and sequentially extracted with a series of solvents that include heptane (Hep), dichloromethane, and methanol. These reports highlight an inverse correlation between H/C and polarity. Acevedo et al.[61] reported the fractionation of asphaltenes by complexation with *p*-nitrophenol and concluded that differences in solubility/aggregation behavior are driven by molecular structure; theoretical calculations demonstrated that island/rigid structures were consistent with low solubility, whereas archipelago/flexible structures agreed with high solubility in Tol.

Several works suggest that extrography is suitable to obtain asphaltene subfractions with different compositions and behaviors. Sjöblom et al.[62] reported a novel fractionation based on the adsorption of asphaltenic samples on $CaCO_3$. In this procedure, an asphaltene solution in Tol is mixed with $CaCO_3$ particles. The non-adsorbed species constitute the non-active fraction. Desorption of asphaltene compounds with tetrahydrofuran (THF) yields a fraction with a moderate interaction with the mineral surface. Finally, the dissolution of the $CaCO_3$ particles with hydrochloric acid produces a fraction of molecules that are irreversibly adsorbed. Adsorption tests of the fractions on stainless steel and aggregation studies demonstrated that the irreversibly adsorbed asphaltenes exhibit higher adsorption/aggregation rates when compared to the non-active fraction; however, extensive oxidation was observed during this procedure.[63] In another report, Romão et al.[64] performed a comparable separation using silica gel to yield non-adsorbed, adsorbed, and irreversibly adsorbed asphaltene fractions. In this report, NMR and high-resolution MS analyses

DOI: 10.1021/acs.energyfuels.7b03281
Energy Fuels 2018, 32, 314−328

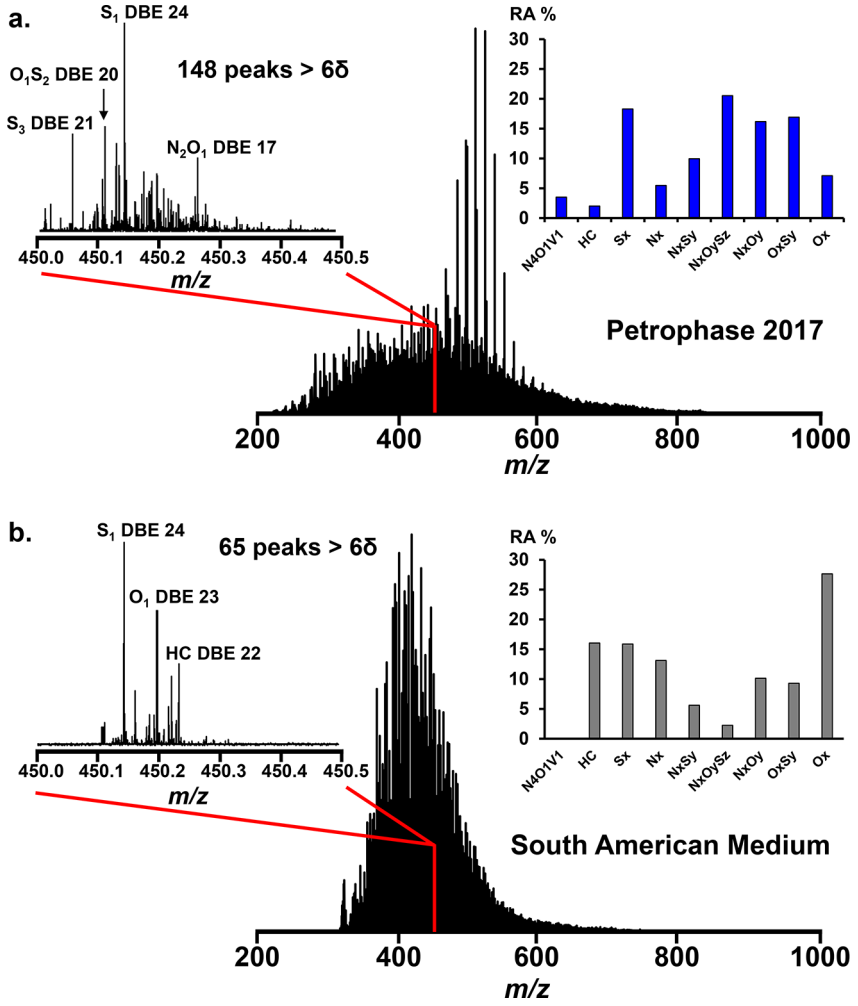

Figure 1. Positive-ion APPI FT-ICR MS mass spectra, with zoomed mass insets at m/z 450 and heteroatom group distributions for (a) whole PetroPhase 2017 asphaltenes and (b) whole South American Medium asphaltenes.

indicated that the adsorption on silica particles is preferential for asphaltene species with a lower content of aromatic hydrogen.

Although there are extensive works related to asphaltene fractionation, most of the structural studies by tandem MS have focused only on whole asphaltene samples. For instance, MS reports on the fragmentation behavior of whole asphaltene samples from different geological origins, by electron impact and collision-induced dissociations, have shown fragmentation pathways that correlate with island structures; the mass losses indicated only loss of alkyl side chains.[18,65−67] The reports have strengthened the prevalent (and incorrect) hypothesis that most asphaltene samples are predominantly composed of island structural motifs.

The work herein focuses on the development of an extrography fractionation method specifically designed to extend the molecular characterization of asphaltenes by MS. Asphaltenes were adsorbed on silica gel and Soxhlet-extracted with two series of solvents to first remove the species that are easily ionized in APPI and then to fractionate the remaining species based on polarity. The mass spectral results are summarized for two asphaltene samples, their eight fractions, and infrared multiphoton dissociation (IRMPD) products to reveal compositional, structural, and associated ionization trends exposed by fractionation.

EXPERIMENTAL SECTION

Materials. High-performance liquid chromatography (HPLC)-grade *n*-heptane (*n*-C_7), dichloromethane (DCM), acetone, acetonitrile (AcCN), Tol, THF, methanol (MeOH), and chromatographic-grade silica gel (100−200 mesh, type 60 Å, Fisher Scientific) were used as received. Whatman filter paper grade 42 and high-purity glass microfiber thimbles were used for Soxhlet extraction (Whatman, GE Healthcare, Little Chalfont, U.K.).

Asphaltene Samples. PetroPhase 2017 asphaltenes were supplied by Total, prepared by the group of professor Marianny Y. Combariza[68] (Universidad Industrial de Santander, Bucaramanga, Colombia), and used as received. South American Medium asphaltenes were precipitated from the crude oil following a standard modified ASTM D6560-12 procedure. In short, 10 g of crude oil was sonicated at 60 °C as 400 mL of *n*-heptane was added dropwise. Then, the mixture was refluxed at 115 °C for 90 min; subsequently, the sample was allowed to stand overnight. Solids were collected by filtration (Whatman grade 42), placed in a Soxhlet apparatus, and Soxhlet-extracted with *n*-heptane until the recycling solvent appeared clear. Asphaltenes were recovered by dissolution in hot Tol (~50 °C), which was finally evaporated under N_2. Subsequently, asphaltenes were subjected to an additional purification process following the method published by Chacón-Patiño et al.[68] Briefly, the purification process includes an initial Soxhlet extraction of asphaltenes with *n*-heptane, followed by grinding with a mortar and pestle and subsequent extraction with fresh *n*-heptane. The grinding followed by Soxhlet extraction was repeated 4 times in 5 h intervals.

DOI: 10.1021/acs.energyfuels.7b03281
Energy Fuels 2018, 32, 314−328

Asphaltene Fractionation. Figure S1 of the Supporting Information illustrates the fractionation process and includes gravimetric results for South American Medium and PetroPhase 2017 asphaltenes. Silica gel was dried overnight at 120 °C prior to adsorption. A total of 20 mg of asphaltenes was dissolved in 400 mL of DCM (25 ug/mL), placed in a round-bottom flask, and mixed with 4 g of silica gel (5 mg of asphaltenes/g of SiO_2). The mixture was stirred at 1500 rpm under N_2 flow until complete solvent evaporation. The composite SiO_2/asphaltenes was placed in a Soxhlet apparatus. The extraction of asphaltene fractions was carried out in eight stages (every 24 h), using the following solvents: acetone, AcCN, Hep, 1:1 Hep/Tol, Tol, 1:1 Tol/THF, THF, and 4:1 THF/MeOH. A justification of stationary phase and solvent selection is discussed in the Results and Discussion. The fractionation process was performed in at least triplicate for each asphaltene sample. All of the fractions were dried under nitrogen, weighed, and stored in the dark for further MS analyses.

Positive-Ion Atmospheric Pressure Photoionization Fourier Transform Ion Cyclotron Resonance Mass Spectrometry [(+) APPI FT-ICR MS]. All asphaltene samples and fractions were dissolved in Tol at a concentration of 200 μg mL^{-1} and directly infused at 50 μL min^{-1}. The samples were analyzed with a custom-built 9.4 T Fourier transform ion cyclotron resonance mass spectrometer, and data collection was facilitated by a modular ICR data acquisition system (PREDATOR).[69,70] Complete mass spectral and tandem (IRMPD) conditions are identical to those previously reported.[32] Molecular formula assignments and data visualization were performed with PetroOrg N-15.0 software.[71]

RESULTS AND DISCUSSION

The characterization of asphaltenes by MS is not a straightforward task as a result of the intrinsic complexity of the samples and the preferential aggregation of specific asphaltene subfractions.[1,55,72] Asphaltenes contain tens of thousands of different species, and the most aromatic species are often preferentially observed by direct infusion APPI MS.[28,35,73] The work presented herein focuses on a separation method that extends the characterization of asphaltenes by MS and the identification of island and archipelago structural motifs. For this purpose, we selected two asphaltene samples that exhibit very different behaviors in direct infusion MS. Figure 1 highlights the compositional differences between the PetroPhase 2017 and South American Medium asphaltenes. The PetroPhase 2017 sample (Figure 1a) exhibits a greater concentration of vanadium (641 ppm) relative to South American Medium asphaltenes, evident by a series of abundant peaks between m/z ~470 and ~650 that correspond to vanadyl porphyrins.[74,75] This asphaltene sample exhibits high spectral complexity, with 148 peaks within a nominal mass at m/z 450, and the ion signals span over low and high mass defects (~0.011000−0.415000), which suggests a high degree of structural diversity.[28] Conversely, the South American Medium asphaltenes (Figure 1b) contain a much lower concentration of vanadium (~16 ppm); thus, no vanadyl porphyrins are observed in the mass spectrum. Furthermore, a single nominal mass zoom inset at m/z 450 shows only 65 peaks, with a narrower distribution of mass defects, indicative of lower compositional complexity.

Molecular formulas, assigned to the mass spectral signals, were sorted by heteroatomic class, hydrogen deficiency [double bond equivalent (DBE)], and alkylation. The heteroatomic class graphs for each sample are shown in Figure 1. The bottom panel of Figure 1 shows that South American Medium asphaltenes are enriched in oxygen-containing compounds (class O_x), exhibit a high relative abundance (~16%) of hydrocarbons (HCs), and do not show the presence of vanadyl porphyrins ($N_4O_1V_1$). On the other hand, PetroPhase 2017 asphaltenes are enriched in sulfur-containing compounds, (classes S_x, $N_xO_yS_z$, and O_xS_y) and vanadyl porphyrins (~3.5% of relative abundance) but depleted in nonpolar HCs. The PetroPhase 2017 asphaltenes also contain a higher content of poly-heteroatomic species that belong to the groups $N_xO_yS_z$ and $N_4O_1V_1$.

Representation of the molecular assignments in contour plots of DBE versus carbon number is useful to visualize the compositional differences between complex samples.[76−79] Figure 2 highlights the asphaltene compositional differences

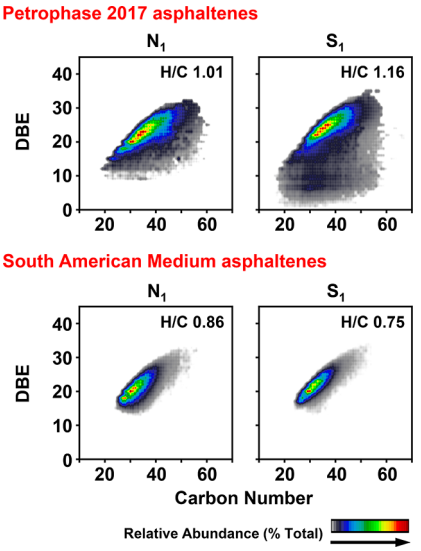

Figure 2. Positive-ion APPI-derived color-contoured isoabundance plots of DBE versus carbon number for N_1 and S_1 heteroatom classes for (top) whole PetroPhase 2017 and (bottom) whole South American Medium asphaltenes.

through DBE versus carbon number plots for the N_1 and S_1 classes from the whole PetroPhase 2017 and South American Medium asphaltene samples. The molecular composition of the PetroPhase 2017 asphaltenes features broader distributions of DBE and carbon number for all classes. Observed ions for South American Medium asphaltenes lie close to the planar aromatic limit, whereas ions observed for PetroPhase 2017 asphaltenes reveal molecular compositions that extend to DBE values much lower than those typically considered for asphaltenes. A shorter homologous series for the South American asphaltenes is indicative of a decreased alkyl substitution (saturated CH_2 moieties attached to the aromatic core) and, hence, lower H/C ratios (included in Figure 2): PetroPhase 2017 asphaltenes have a H/C > 1, whereas South American Medium asphaltenes exhibit greater aromaticity (H/C < 1). Despite the differences, it is important to highlight that both samples overlap in common compositional space between DBE of ~15−28 and carbon numbers of ~25−40, with high relative abundance of species close to the planar aromatic limit line. DBE versus carbon number plots for S_2, N_1O_1, and O_1S_1 heteroatom classes are also shown in Figure S2 of the Supporting Information.

Selection of the Stationary Phase and Solvents. In this work, asphaltenes are fractionated on the basis of their interactions with the active groups of silica gel and the partition into solvents with characteristic solvation strength for polycyclic aromatic hydrocarbons (PAHs)/polar compounds. Silica gel

DOI: 10.1021/acs.energyfuels.7b03281
Energy Fuels 2018, 32, 314−328

was selected as the stationary phase because it offers two advantages for asphaltene separations. First, the most common adsorption mechanisms for silica gel are hydrogen-bonding and ionic interactions, which provide strong retention for polar functionalities within asphaltene compounds.[80−82] Second, it is important to keep in mind that one of the main concerns about the use of mineral surfaces for asphaltene separation is potential oxidation of these species during the fractionation process.[83,84] It is well-documented that the oxidation of adsorbed asphaltenes on pure silica particles, at temperatures between 25 and 75 °C, is insignificant.[85] Oxidation processes on pure SiO_2 require high activation energies (temperatures greater than ∼150 °C). In this work, all solid/liquid extractions were carried out in a Soxhlet apparatus, at temperatures below 45 °C.

In previous work, we discuss the use of the term monomer ion yield to provide a relative measure of monomer ion production between samples. The monomer ion yield is inversely proportional to the time needed to acquire a target number of ions at a given sample concentration; thus, shorter accumulation times to reach a target ion number result in a higher value for the monomer ion yield. Eight solvents were used to separate asphaltene samples into fractions ideal for mass spectral characterization. The fractionation presented herein employs two solvent series to selectively isolate fractions that have different monomer ion yields. The first series consists of acetone and acetonitrile and is used for the selective extraction of compounds with a high monomer ion yield in APPI. Literature reports suggest that acetone is suitable for the selective removal of low-molecular-weight asphaltenes, petroleum porphyrins, and co-precipitated and entrained maltenes within asphaltene aggregates.[59,86,87] Acetone exhibits high selectivity toward extraction of small/*peri*-condensed aromatic ring systems (1−4 fused rings) as a result of its moderate solvating strength for PAHs.[88,89] Acetonitrile assists in the removal of remnant porphyrins, because Giraldo-Dávila et al.[90] and Márquez et al.[91] reported that acetonitrile is useful for the extrography separation of petroleum fractions enriched with vanadyl porphyrins. The compound families mentioned above are easily ionized and restrict the characterization of difficult to ionize asphaltenes by APPI MS.[32]

After the removal of easily ionized (i.e., those compounds with a high monomer ion yield) species (in the acetone and acetonitrile fractions), a standard eluotropic series is used to separate the remnant asphaltenes based on polarity. The second series starts with *n*-heptane, progresses through Tol, and ends with THF/MeOH.[64,82,92] Although the operational definition of asphaltenes excludes solubility in *n*-heptane,[93] the conditions of the C_7 extraction process, temperature at ∼40 °C, and continuous recycling of pure solvent (at extremely low concentration during a given extraction cycle), resulted in the desorption of "low-polarity" asphaltenic species, as Strausz et al.,[94] Chacón-Patiño et al.,[68] and Juyal et al.[95] have previously reported. The increased aromaticity of the next extraction solvent (Tol) yielded two fractions, Hep/Tol and Tol fractions. Lastly, THF was used to solvate polar asphaltene fractions, which increased the mass recovery from the stationary phase.[82,96,97] Thus, three additional fractions (Tol/THF, THF, and THF/MeOH) were obtained.

Purified C_7 Asphaltene Fractions Exhibit a Wide Range of Monomer Ion Yields. The bar graphs in Figure 3 summarize the mass distribution after the fractionation process (left *y* axis) and monomer ion yield (right *y* axis) of the whole and eight asphaltene fractions, as previously described.[32]

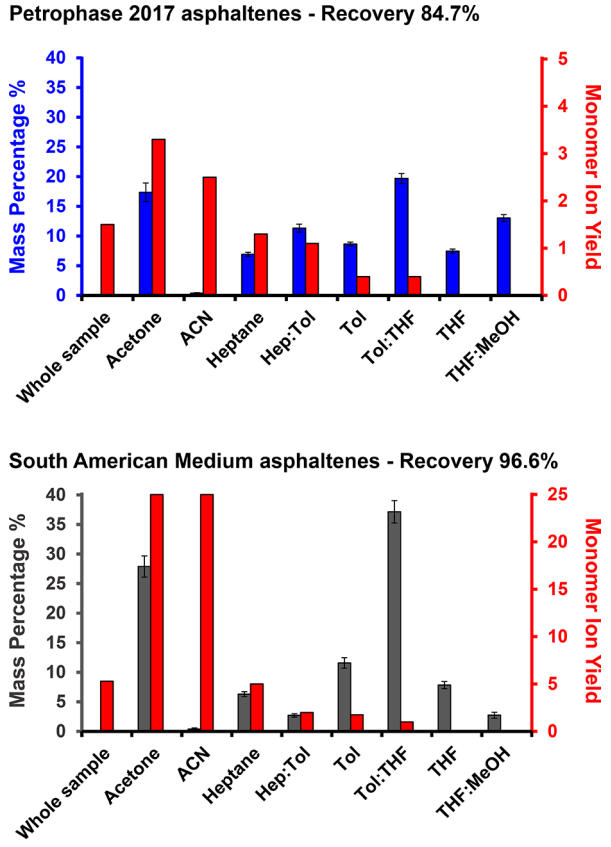

Figure 3. Mass recovery, mass distribution, and monomer ion yield for asphaltene fractionation for (top) PetroPhase 2017 and (bottom) South American Medium asphaltenes.

Mass recoveries are also reported in Table S1 of the Supporting Information. The first major difference between the two asphaltene samples is the total mass recovery. FT-ICR MS analysis of the whole PetroPhase 2017 asphaltene sample (top panel of Figure 1) revealed that it is enriched in polar asphaltenes (polyatomic-containing species) relative to the South American Medium asphaltenes. Thus, it is not surprising that the PetroPhase 2017 sample yielded an 84.7% recovery, as compared to the South American sample that yielded a 96.6% recovery. Analysis of the mass yield for each fraction shows that in both samples, acetone and Tol:THF fractions account for the highest recovered masses. The PetroPhase 2017 asphaltene shows greater yield in the most polar fraction (THF/MeOH) compared to the South American Medium asphaltene and, again, suggests a greater mass of polar asphaltenes in the PetroPhase 2017 sample. Most importantly, only ∼18 wt % of the PetroPhase 2017 sample is recovered in the acetone and ACN fractions, which exhibit a high monomer ion yield, and ∼67 wt % of the sample is recovered with the second solvent series. For both samples, these fractions (Hep−THF/MeOH) exhibit much lower monomer ion yields relative to acetone and ACN fractions.

Table S2 of the Supporting Information includes the accumulation times and the calculated monomer ion yields. Importantly, we found that the final two fractions for each sample (THF and THF/MeOH) were extremely difficult to ionize and were prone to deposit formation in the fused silica capillary just before nebulization. Thus, it was difficult to reliably accumulate the targeted number of ions. Although we were able to successfully analyze the compositional data by FT-

DOI: 10.1021/acs.energyfuels.7b03281
Energy Fuels 2018, 32, 314−328

ICR MS, ionization efficiencies could not be reliably calculated for these samples, and thus, monomer ion yields are not presented for these fractions.

The monomer ion yield is greatest for the acetone and ACN fractions and decreases as the solvent composition progresses toward the Tol/THF fraction. The asphaltene species from the South American Medium sample exhibit a greater monomer ion yield when compared to the species from the PetroPhase 2017 asphaltenes. It is important to highlight that acetone (27.9 wt %) and Tol/THF (37.2 wt %) are the most abundant fractions in the South American Medium asphaltenes but exhibit extreme differences in the monomer ion yield (25 versus 1, respectively). The PetroPhase 2017 sample also reproduces this behavior to a lesser extent: the acetone fraction (17.4 wt %) ionizes ~8 times greater than the Tol/THF fraction (19.7 wt %). It is also worth pointing out that the acetone fractions both showed a greater monomer ion yield than the whole asphaltenes (~2 times greater for PetroPhase 2017 and ~5 times greater for South American Medium); thus, the fractionation method isolated species with a disproportionately high monomer ion yield. The important reason for the 8–25-fold difference in the monomer ion yield between the fractions will be discussed later.

MS of Whole Samples Preferentially Reveals Asphaltene Species That Ionize Most Efficiently. Figure 4 shows

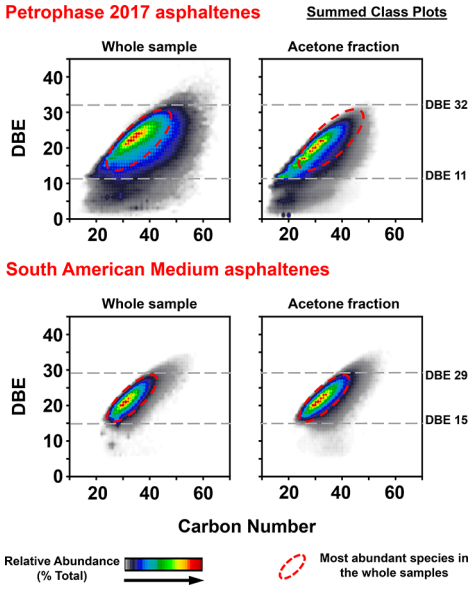

Figure 4. Positive-ion APPI-derived color-contoured isoabundance plots of DBE versus carbon number for all combined compound classes (with percent relative abundance of >0.25, excluding vanadyl porphyrins) from (top) whole asphaltenes and acetone fractions for PetroPhase 2017 and (bottom) whole South American Medium asphaltenes.

the combined DBE versus carbon number plots for all of the compound classes (except for the $N_4O_1V_1$ class) for the whole asphaltenes and the acetone fractions. These results are consistent with the monomer ion yields shown in Figure 3 and indicate that the most ionizable asphaltenes are preferentially observed in the analysis of the whole asphaltene sample. A comparison of the compositional data, mass yields, and monomer ion yields (Figure 3) suggests that direct analysis accesses less than 30 wt % of each whole asphaltene sample analyzed. Thus, ~70 wt % of the whole asphaltene is not detected by direct infusion (dilute and shoot) mass spectral analyses. A future report will demonstrate that this behavior is reproducible for a wide diversity of samples, including virgin and thermally cracked petroleum asphaltenes as well as coal asphaltenes.

Fractionation Accesses Asphaltene Species Not Detected by Direct Infusion. Figure 5 presents the contour plots of DBE versus carbon number for the S_1 class for the extrography fractions from PetroPhase 2017 and South American Medium asphaltenes. The South American Medium asphaltenes (bottom panel of Figure 5) reveal a shift toward higher DBE values through the progression from the acetone to the Tol fraction. Finally, the Tol/THF and THF fractions exhibit a compositional space featured by narrower carbon number distributions, with fewer members per homologous series. This indicates that they have a very low degree of alkyl substitution [methylene units (CH_2) attached to the aromatic cores] in the form of either alkyl chains or naphthenic rings. The PetroPhase 2017 asphaltenes present an interesting contrast to the South American asphaltenes. The acetone fraction from PetroPhase 2017 asphaltenes shows primarily compounds with DBE of >20 and compositional space that spans that of classical, PAH-dominant asphaltene molecules. However, the fractions that elute after the acetone fraction show very atypical asphaltene compositional space. The maximum DBE values similarly increase when moving from acetone to Hep/Tol and Tol fractions; however, the magnitude of the DBE shift is much smaller when compared to South American Medium asphaltenes and is surprisingly accompanied by a widening of the carbon number and DBE ranges. We also note bimodal DBE distributions in the acetonitrile, Hep, Hep/Tol, and Tol fractions that start the atypical compositional space progression for these asphaltene fractions. Further, the Tol/THF fraction exhibits an extremely atypical asphaltene compositional space, with high relative abundance of species with DBE between ~5 and 15 and carbon numbers between ~12 and 40. At first glance, one may assume that these species are remnant occluded maltenes; however, we can rule out this hypothesis based on the following two points: First, the separation with Tol/THF is preceded by extraction (24 h each) with acetone, Hep, and Tol, which are known good solvents for maltenes and would result in the previous extraction of any occluded maltenic-type species. Second, reprecipitation tests with a standard method for asphaltene precipitation[68] were performed and demonstrate that all fractions fit into the operational definition of asphaltenes (Tol soluble but Hep insoluble). In fact, the Tol/THF, THF, and THF/MeOH fractions are difficult to dissolve in Tol and required heating/sonication to achieve complete dissolution. Specifically, 50 mg of the Tol/THF fraction was dissolved in 5 mL of Tol and mixed with 200.0 mL of Hep (40:1 Hep/Tol, with C_7 added dropwise under sonication). These experiments resulted in 99.3 ± 0.5 wt % of the Tol/THF fraction being recovered as C_7 insolubles. Lastly, this odd compositional space behavior is heteroatom-specific (to S_x species) and agrees with results reported by Romão et al.,[64] who performed fractionation of asphaltenes based on adsorption on silica gel. The authors pointed out the irreversible adsorption of the asphaltene species with the lowest content of aromatic hydrogen. For reference, DBE versus carbon number plots for N_1, O_1, S_2, HC, and S_1O_1 classes are provided in Figures S3–S7 of the Supporting Information. Finally, it is important to highlight that the latest fractions (THF and THF/MeOH) exhibit compositional

DOI: 10.1021/acs.energyfuels.7b03281
Energy Fuels 2018, 32, 314–328

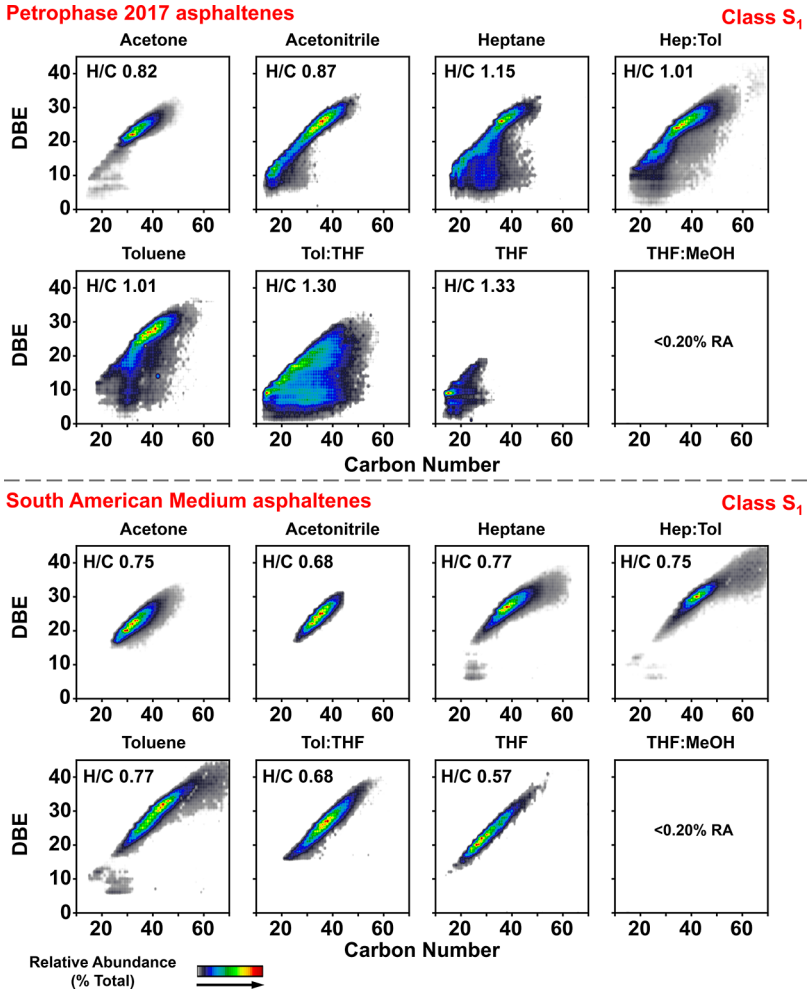

Figure 5. Positive-ion APPI-derived color-contoured isoabundance plots of DBE versus carbon number for S_1 heteroatom class for (top) silica gel fractions from PetroPhase 2017 and (bottom) whole South American Medium asphaltenes.

spaces that do not follow the trend established by earlier fractions. The MS analysis of these fractions was particularly difficult. We hypothesize that the issues with MS analysis of these species was due to aggregation, because they formed capillary deposits (precipitated) during mass spectral analysis. Current efforts are focused on similar advances in MS characterization of these problematic fractions.

Discussion of the composition of each fraction provides an opportunity to point out several subtleties that are important in the current study. As we discussed previously, the unorthodox order of elution solvent provides a separation that is likely based on the structural motif as well as polarity. On the basis of previously published literature[59] as well as monomer ion yields, we believe that the compounds found in the acetone fraction are less likely to aggregate when compared to the other fractions (discussed in more detail later). With this in mind, identical formulas that appear in multiple fractions are likely isomers that are separated on the basis of structural differences that, in turn, influence aggregation tendencies (e.g., compounds with the elemental formula $C_{30}H_{23}N_1$ that are observed in acetone and Tol/THF fractions will likely have different structural motifs and/or functionalities that contribute to the difference in elution). Furthermore, compounds from the PetroPhase 2017 sample that elute with Tol/THF and THF show highly alkylated and low DBE composition that are uncharacteristic of "classical" asphaltenes. However, these low DBE compounds were unique to only the heteroatomic classes that possess sulfur. Figure 6 shows the combined DBE versus carbon number data for all sulfur-containing heteroatom classes (i.e., S_x, N_xS_y, O_xS_y, and $N_xO_yS_z$) as well as the heteroatom classes that do not contain sulfur (i.e., HC, N_x, O_x, and N_xO_y). All S-containing compounds for the PetroPhase 2017 asphaltene show a prominent signature of low DBE (1−4) compounds, whereas S-containing compounds from South American Medium asphaltenes do not. This suggests that the chemistry of sulfur compounds present in each sample is different, and the extremely low DBE values (even below that of thiophene) indicate that the PetroPhase asphaltenes must contain non-aromatic forms of sulfur, such as sulfides and/or thiols.

Progression of Atomic Ratios. Figure 7 includes the relative abundance weighted average of the atomic ratios O/C, S/C, and N/C for the asphaltene samples and extrography fractions. The acetone fractions closely resemble the heteroatom content of the whole asphaltenes for both samples, as obtained by mass spectral analysis. The result supports one of the most important conclusions of this work: mass spectrometric analysis of whole asphaltenes reveals only the species that ionize most efficiently. As a result, atomic ratios derived from FT-ICR MS do not necessarily reflect bulk elemental analyses.[1,98] However, O/C ratios can be used as a proxy for the polarity of the fractions. As the separation procedure with

DOI: 10.1021/acs.energyfuels.7b03281
Energy Fuels 2018, 32, 314−328

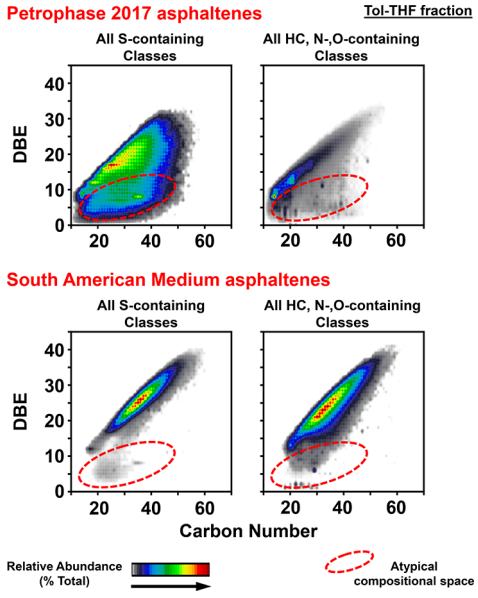

Figure 6. Positive-ion APPI-derived color-contoured isoabundance plots of DBE versus carbon number for S-containing compounds and HC and N- and O-containing compounds from (top) Tol/THF fractions of PetroPhase 2017 and (bottom) whole South American Medium asphaltenes.

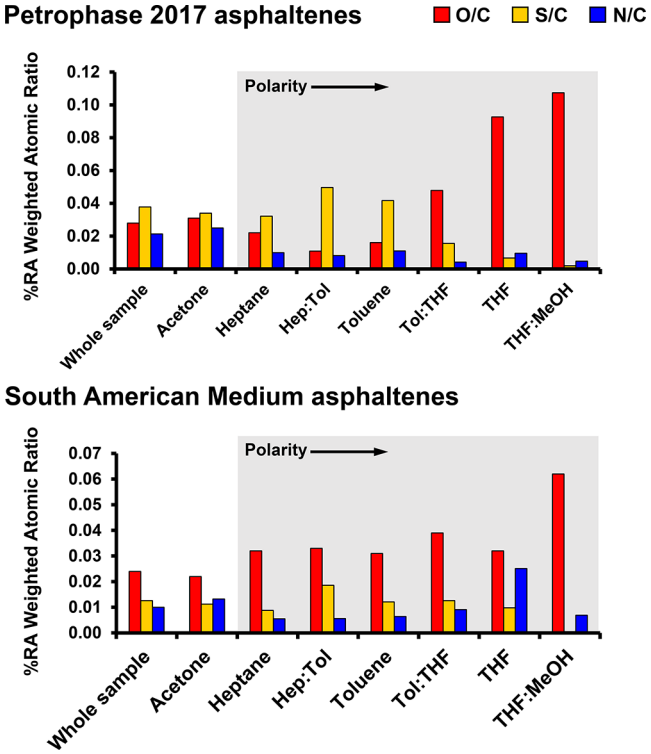

Figure 7. Progression of relative abundance weighted O/C, S/C, and N/C for (top) whole asphaltene samples and corresponding extrography fractions for PetroPhase 2017 and (bottom) whole South American Medium asphaltenes.

the second series of solvents advances, the O/C ratios increase dramatically. The effect is prominent for the PetroPhase 2017 asphaltenes and suggests that polarity plays an important role in the adsorption mechanism on the silica surface, which is not surprising given the previous discussion of mass recovery. On the other hand, the trends for the S/C ratios suggest that S-containing functionalities do not contribute to the strong adsorption of the THF/MeOH fractions. Interestingly, the Hep/Tol fractions from both samples, which present the highest DBE values, exhibit the maximum S/C ratios. Finally, the nitrogen content does not appear to have a clear role in asphaltene adsorption on SiO_2. These results agree with previous reports of asphaltene adsorption on polar surfaces, which suggest that the high content of oxygen correlates with a strong adsorption behavior, whereas sulfur and nitrogen do not appear to have an important effect on the asphaltene interaction with polar surfaces.[99−102]

IRMPD Fragmentation Reveals Fraction Dependence of Island versus Archipelago Structural Motifs. Fractionation of asphaltene samples reveals compositional space changes (DBE versus carbon number) between the fractions and links the monomer ion yields to their order of elution from silica gel. However, the chemical/structural rationale for the wide variation in ionization efficiencies exhibited by the fractions has not been directly explained. We hypothesize that the differences between fractions is likely due to differences in the molecular architecture (island versus archipelago) and/or asphaltene polarity, indicated in Figures 1 and 7. Although the polarity of each sample is easily understood on the basis of the order of elution and oxygen content, the chemical structure is a much more elusive determination. FT-ICR MS provides the unique ability to isolate a small number of mass-defined ions and investigate their changes in elemental composition upon fragmentation. Here, we use IRMPD to fragment mass-selected ranges of ions trapped in the ICR cell prior to detection. The ultrahigh resolution of FT-ICR MS provides the ability to assign chemical formulas to both the parent and fragment ions. Thus, changes in class, DBE, and carbon number can be readily determined. Figure 8 shows the IRMPD fragmentation of the whole PetroPhase 2017 (left panel of Figure 8) and whole South American Medium (right panel of Figure 8) asphaltenes. Mass segments from m/z 453 to 457 were isolated via mass-resolving quadrupole prior to irradiation with an infrared laser. The fragmentation spectra for each sample are shown in the top of Figure 8. The fragmentation of asphaltenes results in two distinct fragment regions. For the mass segment shown here, ions at m/z approximately greater than 350 show a dealkylation pattern (loss of carbon with no loss of aromaticity) and, thus, correspond to island-type fragments, whereas the distribution of peaks from m/z 100 to 350 are lower DBE and carbon number fragments that result from the dissociation of archipelago compounds. The fragmentation of asphaltenes and asphaltene model compounds is discussed in greater depth in the first part of this series (10.1021/acs.energyfuels.7b02873).[32] The PetroPhase 2017 asphaltene exhibits a large number of island- and archipelago-derived fragments, whereas the South American Medium asphaltene reveals primarily island-derived fragments. This can be further shown by DBE versus carbon number plots (bottom panels of Figure 8). Here, we have grouped the HC and mono-heteroatomic classes into one plot and the poly-heteroatomic classes into another plot. We have also included an orange dotted line that indicates the lower DBE limit associated with island fragments. These values are the weighted average of DBE values for the parent ions minus the weighted standard deviation. Fragments with DBE values below this boundary are products formed by the loss of DBE and are due to archipelago structures.

DOI: 10.1021/acs.energyfuels.7b03281
Energy Fuels 2018, 32, 314−328

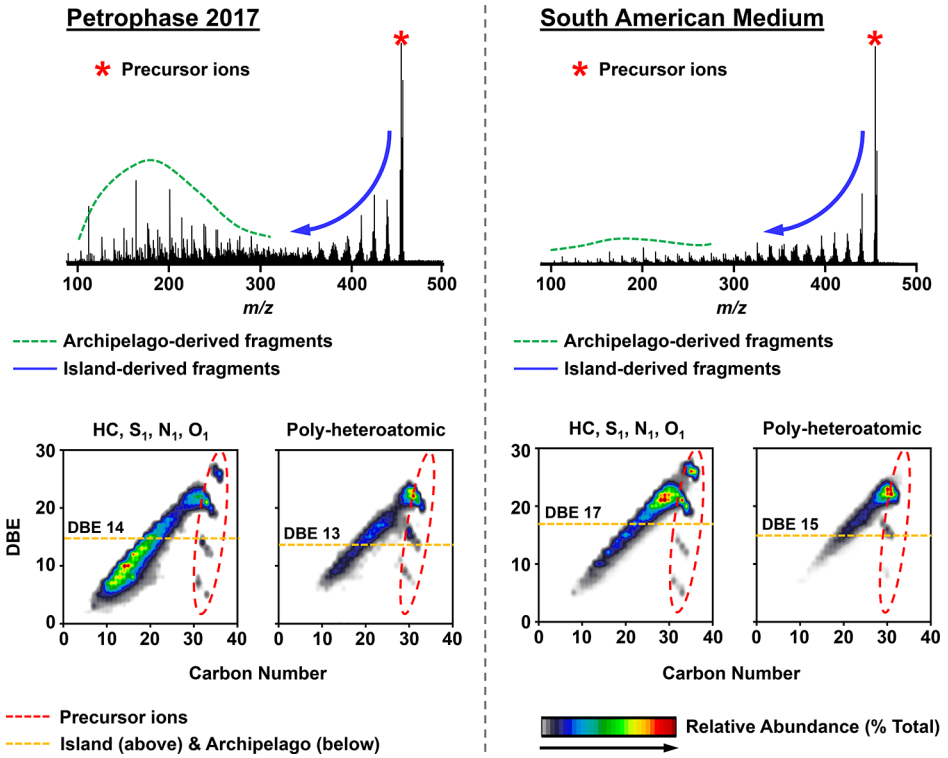

Figure 8. Fragmentation spectra and combined color-contoured isoabundance plots of DBE versus carbon number for (left) precursor and fragment ions from PetroPhase 2017 and (right) whole South American Medium asphaltenes.

Although island and archipelago fragments are observed from the analysis of the whole asphaltene, chemical separation allows us to probe deeper into the compositional complexity through the targeted removal of species that have a disproportionately high monomer ion yield. Figure 9 shows the fragmentation spectra for each extrography fraction for the PetroPhase 2017 asphaltene. Here, we see that the acetone fraction is enriched with island-derived fragments, where dealkylated products are the most abundant. However, as we progress to later-eluting fractions, there is a clear shift to more archipelago fragments, and in the final fractions, only archipelago-derived fragments are observed. We also see that the survival yield of the parent ions (highlighted by a red star) tends to decrease with the increased abundances of archipelago-derived fragments. Figure 10 reveals a more detailed picture of fragments produced for acetone, Hep/Tol, and Tol fractions from PetroPhase 2017 asphaltenes. The DBE versus carbon number plots again show the orange line associated with the archipelago versus island boundary, as discussed above. DBE distributions are also shown in the form of bar graphs for each fraction. Here, each bar is the combination of the relative abundance of the precursor (red) and fragment (gray) ions. For example, when looking at the acetone fraction, the relative abundance of parent ions at DBE of 26 is ∼19% and the relative abundance of fragment ions at DBE of 26 is ∼2%. Therefore, the total bar height is ∼21%. Here, even the acetone fraction shows a high relative abundance of fragments with DBE of less than 17, which indicates the presence of archipelago structures. However, we also see the appearance of fragments with DBE of >20 that reflect the presence of island compounds. As we move to later-eluting fractions, there is a shift in the DBE distributions and the overwhelming majority of fragment ions are observed below the archipelago DBE boundary. Figure 11 shows the fragmentation spectra for South American Medium asphaltene fractions. Recall that similar analysis of the whole, unfractionated sample yielded island-dominant structures. As expected, the acetone fraction (high monomer ion yield) reveals almost exclusively island-derived fragments; however, the presence of archipelago-derived fragments starts to appear in the ACN and Hep fractions. We also see that the latest three fractions reveal almost exclusively archipelago-derived fragments. The South American Medium asphaltenes have a high survival yield of molecular ion for the earliest-eluting fractions, which again show the enrichment in island-derived fragments. Figure 12 shows the DBE versus carbon number plots and DBE distributions for the South American Medium asphaltenes. South American Medium asphaltenes show a greater contribution from island structural motifs in the acetone fraction, where the majority of fragment ions are observed at DBE values greater than the island versus archipelago boundary. The Hep/Tol fraction also shows the presence of mostly island-derived fragments; however, the Tol/THF fraction shows the presence of large quantities of archipelago-derived fragments. Here, the Tol/THF fraction was chosen because it is the earliest eluting fraction that exhibits substantial production of archipelago fragments. The most abundant parent ions are located at DBE of 25 and 26, whereas the most abundant fragment ions are at DBE of 6. Three very important conclusions may be drawn from this work. First, fractionation of asphaltenes by extrography shows that archipelago fragments are observed, even for a sample that shows primarily island-type fragments from the whole asphaltene. Second, the enrichment of island-derived fragments in the acetone fraction and archipelago-derived fragments in the Tol/THF, THF, and THF/MeOH fractions indicates that the samples are being fractionated by the structure (island and archipelago motifs). Third, high relative abundance of archipelago fragments in late-eluting fractions corresponds to fractions with the lowest

DOI: 10.1021/acs.energyfuels.7b03281
Energy Fuels 2018, 32, 314−328

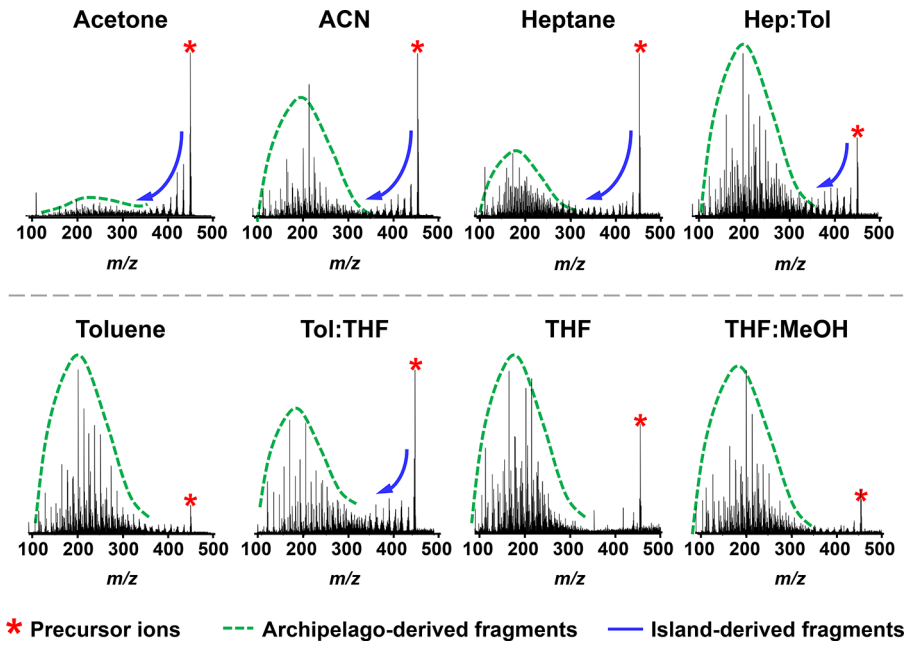

Figure 9. Fragmentation spectra for extrography fractions from PetroPhase 2017 asphaltenes.

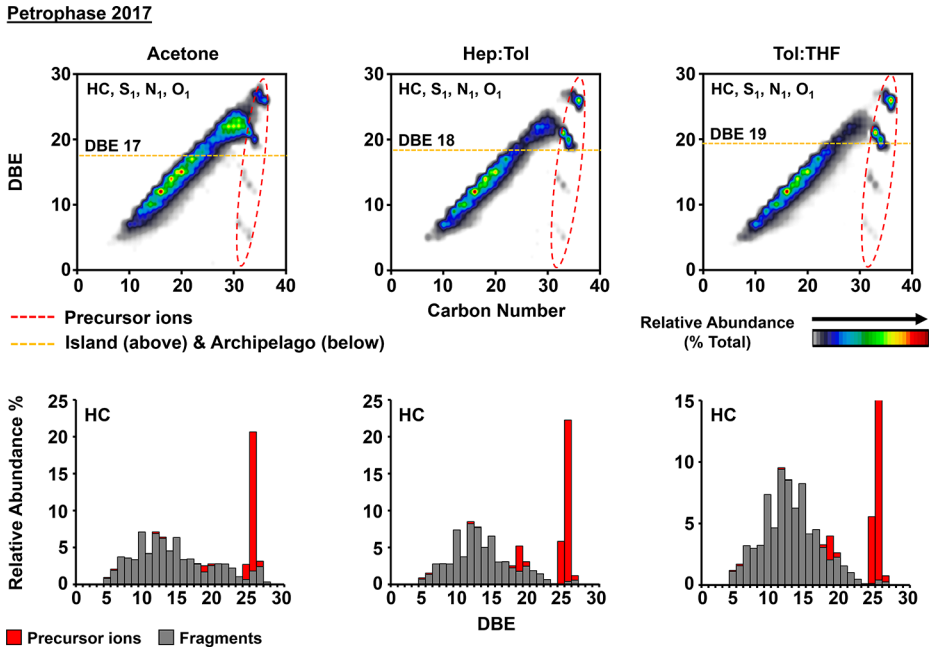

Figure 10. Combined color-contoured isoabundance plots of DBE versus carbon number for precursor and fragment ions and DBE distributions for precursor and fragment ions from PetroPhase 2017 asphaltenes.

monomer ion yield. This indicates, as we proposed in the first work of this series (10.1021/acs.energyfuels.7b02873), that the monomer ion yield is likely linked to aggregation tendency and that archipelago compounds aggregate to a much greater extent than island compounds.

Mass Dependence of Structural Motif. Until now, we have discussed fragments from only one mass range. However, to properly understand the composition of asphaltenes, several molecular weight ranges must be interrogated. Figure 13 shows the fragmentation spectra, DBE versus carbon number plots, and DBE distributions for the acetone fraction from South American Medium asphaltenes. The orange line in DBE versus carbon number plots indicates the boundary for island and archipelago fragments, as discussed above. Recall that this is the fraction that is isolated from the sample that shows the greatest contribution from island-derived fragments. Fragments from m/z 453 to 457 show primarily an island structural motif, and the majority of fragments reveal DBE values of >18. An increase of ~100 Da reveals a dramatic increase in low DBE (archipelago) fragments, with similar relative abundances for ions less than and greater than DBE of 21 (near equal island and archipelago contents). The final increase in molecular weight, to m/z 651−655, reveals that the majority of ions have DBE values of <22, which indicates a greater contribution from archipelago-derived fragments. Thus, archipelago structures are

DOI: 10.1021/acs.energyfuels.7b03281
Energy Fuels 2018, 32, 314−328

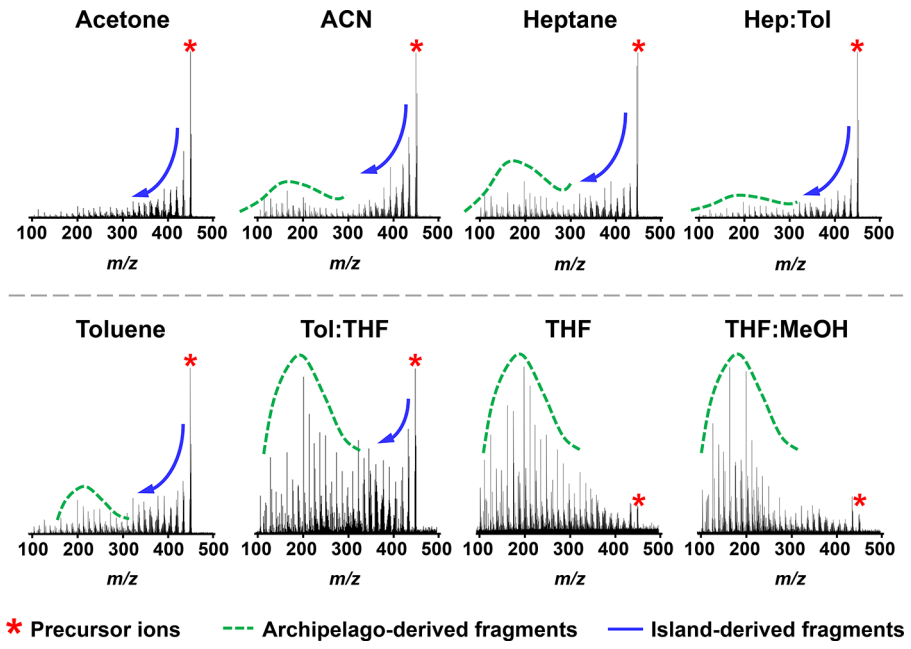

Figure 11. Fragmentation spectra for extrography fractions from South American Medium asphaltenes.

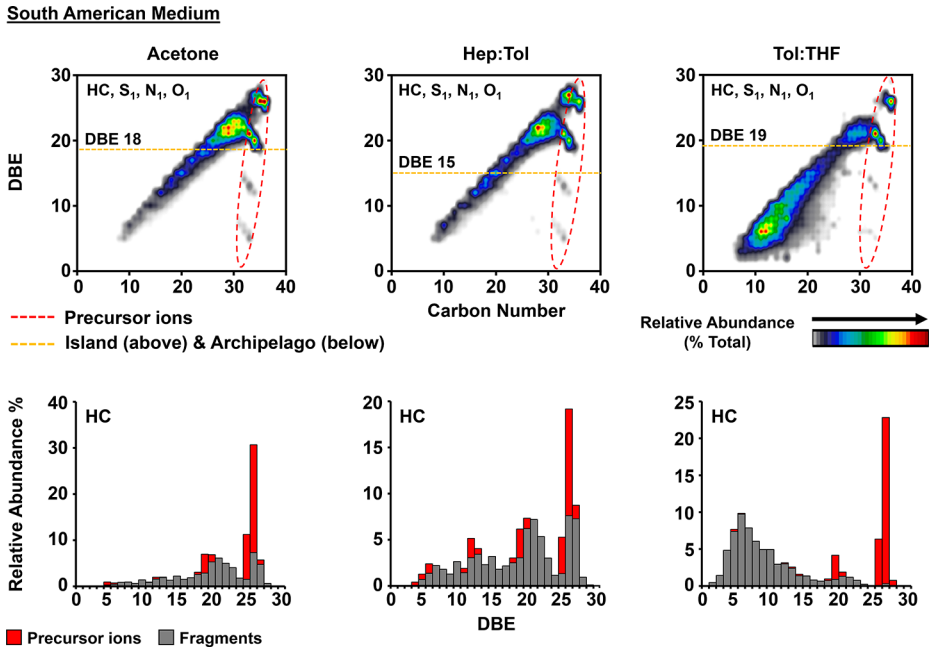

Figure 12. Combined color-contoured isoabundance plots of DBE versus carbon number for precursor and fragment ions and DBE distributions for precursor and fragment ions from South American Medium asphaltenes.

more abundant as the carbon number and DBE increase, even in a fraction enriched in island-type structural motifs.

FUTURE DIRECTIONS: LINK BETWEEN COMPOSITION AND BEHAVIOR

The work presented herein highlights the power of FT-ICR MS combined with separation techniques to glean structural and chemical information for what is arguably one of the most complex mixtures known. The insight into chemical composition and molecular structure compounded with the ability to observe difficult to ionize fractions provides a greater compositional understanding for asphaltene samples. Herein, we propose a correlation between the monomer ion yield and structure, presumably as a result of aggregation tendency. Island structures have a lower tendency to self-associate than archipelago structures, and thus, they ionize efficiently as monomeric species. Archipelago species self-associate more than island structures and, as a result, have lower ionization yields of asphaltene monomers. However, the ultimate goal of petroleomics is to correlate molecular-level composition to behavior. To that end, we analyzed the precipitation behavior of the whole PetroPhase 2017 asphaltenes and compared it to two of the isolated fractions [acetone (island dominant) and Tol/THF (archipelago dominant)]. Figure 14 shows the dramatic difference in the mass of precipitated asphaltenes when titrated with *n*-heptane. For the whole asphaltene, ~20 wt % of the

DOI: 10.1021/acs.energyfuels.7b03281
Energy Fuels 2018, 32, 314−328

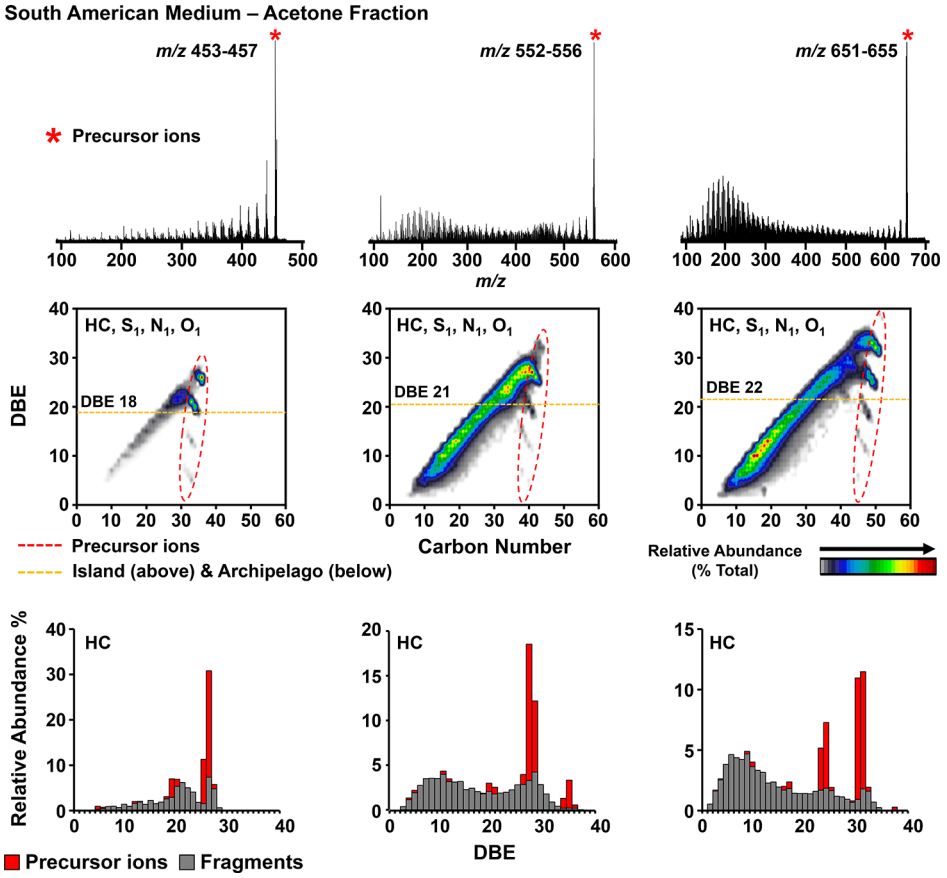

Figure 13. Fragmentation spectra, combined color-contoured isoabundance plots of DBE versus carbon number for precursor and fragment ions, and DBE distributions for precursor and fragment ions for m/z (left) 453−457, (middle) 552−556, and (right) 651−655 for the acetone fraction from South American Medium asphaltenes.

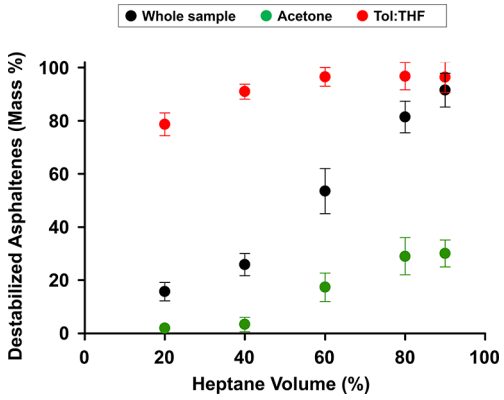

Figure 14. Precipitation mass percentage versus titrated volume percentage of Hep in Tol solution for the whole PetroPhase 2017 asphaltenes and the corresponding acetone and Tol/TFH fractions.

sample is precipitated with 20 vol % *n*-heptane. At 60 vol % Hep, ∼54 wt % is recovered, and the addition of 90 vol % Hep results in ∼91 wt % precipitated. Conversely, the island-dominant acetone fraction, which ionized with the greatest efficiency, shows no appreciable precipitation at 20 vol % Hep and only ∼30 wt % precipitation at 90 vol % Hep. The acetone fraction, which is island-dominant, does not precipitate as readily as the whole sample and is more stable throughout Hep titration. The archipelago dominant Tol/THF fraction had the lowest monomer ion yield of the fractions measured and shows 80 wt % precipitation at only 20 vol % Hep. Furthermore, the Tol/THF fraction shows complete precipitation (96 wt %) at Hep volume percentages greater than 60%. Thus, these results suggest that ionization and aggregation/precipitation in normal paraffin solvents are correlated. Most surprisingly, the archipelago fraction of asphaltenes, which is difficult to observe by (+) APPI FT-ICR MS without prior fractionation and was thought to be a minor mass fraction, accounts for a disproportionately large fraction of asphaltene instability in Hep dilution. Further work will be conducted to further investigate this and other potential correlations to behavior.

CONCLUSION

An extrography fractionation method was specifically designed to extend the molecular characterization of asphaltenes by APPI MS. Asphaltenes were adsorbed on silica gel and Soxhlet-extracted with two series of solvents. The first consists of acetone and acetonitrile and is used for the selective removal of asphaltene species that exhibit a disproportionately high monomer ion yield by APPI. The second series of solvents is a polarity gradient and uses *n*-heptane, Tol, THF, and methanol to separate asphaltenes based on solubility. The proposed method was demonstrated on two compositionally different asphaltenes, a South American Medium asphaltene and the PetroPhase 2017 asphaltene, after extensive purification to remove entrained/occluded maltenes. A total of eight fractions were collected, and the earliest eluting fraction (acetone fraction) ionized most efficiently and matched the MS results obtained for the whole (unfractionated) asphaltenes. The

DOI: 10.1021/acs.energyfuels.7b03281
Energy Fuels 2018, 32, 314−328

acetone fraction also exhibited enrichment of island motifs when analyzed by (+) APPI FT-ICR MS with IRMPD. The analysis of fractions 3−8 (lower monomer ion yield) revealed asphaltene compounds that were not observed in the whole asphaltene sample and thereby greatly extended the number of assigned species. The selective removal of asphaltenic species with a high monomer ion yield (in the acetone and acetonitrile fractions) reveals difficult to ionize species (~70 wt % of each sample) that, after IRMPD, exhibit dominant fragmentation patterns that are possible only for archipelago structural motifs. Fractions 3−6 exhibited ~10−25-fold lower monomer ion yields than the acetone fractions, which was evident by the longer ion accumulation times required for the commensurate mass spectral signal-to-noise ratio. Thus, direct analysis of the whole asphaltene samples fails to detect these species. IRMPD of three different (increasing) mass ranges revealed that the proportion of archipelago-type fragments increases with increasing mass, even in the most island-dominant fraction, of the most island-dominant asphaltene sample (South American Medium). The poor ionization of the later-eluting fractions (3−6) was found to be correlated to the presence of increased levels of archipelago-type fragments. Hep titration of the whole asphaltene, acetone fraction (island dominant), and Tol/THF fraction (archipelago dominant) revealed that the acetone fraction was significantly more stable than the whole asphaltene and that the Tol/THF fraction was dramatically more unstable than both the acetone and whole asphaltene samples. In combination, these results suggest that the decreased monomer ion yield of later-eluting fractions is due to their tendency to self-associate and that this tendency is structure-dependent; the fragmentation of later-eluting fractions exposes a predominance of archipelago structures.

■ ASSOCIATED CONTENT

Supporting Information

The Supporting Information is available free of charge on the ACS Publications website at DOI: 10.1021/acs.energyfuels.7b03281.

Mass distribution and recovery percentage for PetroPhase 2017 and South American Medium asphaltenes (Table S1), ionization efficiency calculations for whole and fractionated asphaltene samples (Table S2), and figure captions for Figures S1−S7 (PDF)

Summary of the fractionation procedure along with the gravimetric yields of each fraction for the PetroPhase 2017 and South American Medium asphaltene samples (Figure S1) (PDF)

DBE versus carbon number plots for the classes N_1, S_1, S_2, N_1O_1, and O_1S_1 for the whole (top) PetroPhase 2017 and (bottom) South American Medium asphaltene samples obtained by APPI FT-ICR MS, with the abundance weighted H/C ratio given for each plot (Figure S2) (PDF)

DBE versus carbon number plots for the class N_1 for all eight fractions from (top) PetroPhase 2017 and (bottom) South American Medium asphaltenes obtained by APPI FT-ICR MS (Figure S3) (PDF)

DBE versus carbon number plots for the class O_1 for all eight fractions from (top) PetroPhase 2017 and (bottom) South American Medium asphaltenes obtained by APPI FT-ICR MS (Figure S4) (PDF)

DBE versus carbon number plots for the HC class for all eight fractions from (top) PetroPhase 2017 and (bottom) South American Medium asphaltenes obtained by APPI FT-ICR MS (Figure S5) (PDF)

DBE versus carbon number plots for the class O_1S_1 for all eight fractions from (top) PetroPhase 2017 and (bottom) South American Medium asphaltenes obtained by APPI FT-ICR MS (Figure S6) (PDF)

DBE versus carbon number plots for the class S_2 for all eight fractions from (top) PetroPhase 2017 and (bottom) South American Medium asphaltenes obtained by APPI FT-ICR MS (Figure S7) (PDF)

■ AUTHOR INFORMATION

Corresponding Authors

*Telephone: +1-850-644-1319. Fax: +1-850-644-1366. E-mail: rowland@magnet.fsu.edu.

*Telephone: +1-850-644-2398. Fax: +1-850-644-1366. E-mail: rodgers@magnet.fsu.edu.

ORCID

Ryan P. Rodgers: 0000-0003-1302-2850

Notes

The authors declare no competing financial interest.

■ ACKNOWLEDGMENTS

This work was supported by the National Science Foundation (NSF) Division of Materials Research (DMR-1157490), the Florida State University, the Florida State University Future Fuels Institute, and the State of Florida. The authors thank Don F. Smith and Greg Blakney for help with data calibration and instrument performance and Yuri E. Corilo for PetroOrg software. The authors also thank Logan C. Krajewski for help with laser alignment for IRMPD experiments. The authors give a special thanks to Marianny Y. Combariza for providing the South American crude oil and Pierre Giusti and the organizers of PetroPhase 2017 for providing the PetroPhase 2017 asphaltene.

■ REFERENCES

(1) Purcell, J. M.; Merdrignac, I.; Rodgers, R. P.; Marshall, A. G.; Gauthier, T.; Guibard, I. *Energy Fuels* **2010**, *24*, 2257−2265.

(2) Herod, A. A. *Rapid Commun. Mass Spectrom.* **2010**, *24*, 2507−2519.

(3) Herod, A. A.; Bartle, K. D.; Morgan, T. J.; Kandiyoti, R. *Chem. Rev.* **2012**, *112*, 3892−3923.

(4) Tavakkoli, M.; Panuganti, S. R.; Taghikhani, V.; Pishvaie, M. R.; Chapman, W. G. *Fuel* **2014**, *117*, 206−217.

(5) Buckley, J. S. *Energy Fuels* **2012**, *26*, 4086−4090.

(6) Molina Velasco, D.; Ariza Leon, E.; Chaves-Guerrero, A. *Energy Fuels* **2017**, *31*, 8997−9005.

(7) Eskin, D.; Mohammadzadeh, O.; Akbarzadeh, K.; Taylor, S. D.; Ratulowski, J. *Can. J. Chem. Eng.* **2016**, *94*, 1202−1217.

(8) Sjöblom, J.; Hemmingsen, P. V.; Kallevik, H. *Asph. Heavy Oils, Pet.* **2007**, 549−587.

(9) Stark, J. L.; Asomaning, S. *Pet. Sci. Technol.* **2003**, *21*, 569−579.

(10) Rodgers, R. P.; Schaub, T. M.; Marshall, A. G. *Anal. Chem.* **2005**, *77*, 20 A−27 A.

(11) Strausz, O. P.; Mojelsky, T. W.; Lown, E. M. *Fuel* **1992**, *71*, 1355−1363.

(12) Mullins, O. C.; Sabbah, H.; Eyssautier, J.; Pomerantz, A. E.; Barré, L.; Andrews, A. B.; Ruiz-Morales, Y.; Mostowfi, F.; McFarlane, R.; Goual, L.; Lepkowicz, R.; Cooper, T.; Orbulescu, J.; Leblanc, R. M.; Edwards, J.; Zare, R. N. *Energy Fuels* **2012**, *26*, 3986−4003.

DOI: 10.1021/acs.energyfuels.7b03281
Energy Fuels 2018, 32, 314−328

(13) Alvarez-Ramírez, F.; Ruiz-Morales, Y. *Energy Fuels* **2013**, *27*, 1791−1808.
(14) Mullins, O. C. *Annu. Rev. Anal. Chem.* **2011**, *4*, 393−418.
(15) Mullins, O. C. *Energy Fuels* **2010**, *24*, 2179−2207.
(16) Schuler, B.; Meyer, G.; Peña, D.; Mullins, O. C.; Gross, L. *J. Am. Chem. Soc.* **2015**, *137*, 9870−9876.
(17) Groenzin, H.; Mullins, O. C. *J. Phys. Chem. A* **1999**, *103*, 11237−11245.
(18) Tang, W.; Hurt, M. R.; Sheng, H.; Riedeman, J. S.; Borton, D. J.; Slater, P.; Kenttämaa, H. I. *Energy Fuels* **2015**, *29*, 1309−1314.
(19) Rueda-Velásquez, R. I.; Freund, H.; Qian, K.; Olmstead, W. N.; Gray, M. R. *Energy Fuels* **2013**, *27*, 1817−1829.
(20) Karimi, A.; Qian, K.; Olmstead, W. N.; Freund, H.; Yung, C.; Gray, M. R. *Energy Fuels* **2011**, *25*, 3581−3589.
(21) Karimi, A.; Qian, K.; Olmstead, W. N.; Freund, H.; Yung, C.; Gray, M. R. *Energy Fuels* **2011**, *25*, 3581−3589.
(22) Gray, M. R. *Energy Fuels* **2003**, *17*, 1566−1569.
(23) Savage, P. E.; Klein, M. T.; Kukes, S. G. *Prepr. Pap. - Am. Chem. Soc., Div. Fuel Chem.* **1985**, *30*, 408−419.
(24) Alshareef, A. H.; Scherer, A.; Tan, X.; Azyat, K.; Stryker, J. M.; Tykwinski, R. R.; Gray, M. R. *Energy Fuels* **2012**, *26*, 1828−1843.
(25) Sheremata, J. M.; Gray, M. R.; Dettman, H. D.; McCaffrey, W. C. *Energy Fuels* **2004**, *18*, 1377−1384.
(26) Podgorski, D. C.; Corilo, Y. E.; Nyadong, L.; Lobodin, V. V.; Bythell, B. J.; Robbins, W. K.; McKenna, A. M.; Marshall, A. G.; Rodgers, R. P. *Energy Fuels* **2013**, *27*, 1268−1276.
(27) Sabbah, H.; Morrow, A. L.; Pomerantz, A. E.; Zare, R. N. *Energy Fuels* **2011**, *25*, 1597−1604.
(28) McKenna, A. M.; Marshall, A. G.; Rodgers, R. P. *Energy Fuels* **2013**, *27*, 1257−1267.
(29) Itoh, N.; Aoyagi, Y.; Yarita, T. *J. Chromatogr. A* **2006**, *1131*, 285−288.
(30) Robb, D. B.; Covey, T. R.; Bruins, a P. *Anal. Chem.* **2000**, *72*, 3653−3659.
(31) Rogel, E.; Moir, M.; Witt, M. *Energy Fuels* **2015**, *29*, 4201−4209.
(32) Chacón-Patiño, M. L.; Rowland, S. M.; Rodgers, R. P. *Energy Fuels* **2017**, DOI: 10.1021/acs.energyfuels.7b02873.
(33) Gray, M.; Tykwinski, R.; Stryker, J.; Tan, X. *Energy Fuels* **2011**, *25*, 3125−3134.
(34) Andreatta, G.; Bostrom, N.; Mullins, O. C. *Langmuir* **2005**, *21*, 2728−2736.
(35) McKenna, A. M.; Donald, L. J.; Fitzsimmons, J. E.; Juyal, P.; Spicer, V.; Standing, K. G.; Marshall, A. G.; Rodgers, R. P. *Energy Fuels* **2013**, *27*, 1246−1256.
(36) Pomerantz, A. E.; Hammond, M. R.; Morrow, A. L.; Mullins, O. C.; Zare, R. N. *J. Am. Chem. Soc.* **2008**, *130*, 7216−7217.
(37) Pomerantz, A. E.; Hammond, M. R.; Morrow, A. L.; Mullins, O. C.; Zare, R. N. *Energy Fuels* **2009**, *23*, 1162−1168.
(38) Sabbah, H.; Morrow, A. L.; Pomerantz, A. E.; Mullins, O. C.; Tan, X.; Gray, M. R.; Azyat, K.; Tykwinski, R. R.; Zare, R. N. *Energy Fuels* **2010**, *24*, 3589−3594.
(39) Sabbah, H.; Morrow, A. L.; Pomerantz, A. E.; Zare, R. N. *Energy Fuels* **2011**, *25*, 1597−1604.
(40) Castillo, J.; Vargas, V. *Pet. Sci. Technol.* **2016**, *34*, 873−879.
(41) Rowland, S. M.; Robbins, W. K.; Corilo, Y. E.; Marshall, A. G.; Rodgers, R. P. *Energy Fuels* **2014**, *28*, 5043−5048.
(42) Honse, S. O.; Ferreira, S. R.; Mansur, C. R. E.; Lucas, E. F.; González, G. *Quim. Nova* **2012**, *35*, 1991−1994.
(43) Cho, Y.; Na, J.; Nho, N.; Kim, S.; Kim, S. *Energy Fuels* **2012**, *26*, 2558−2565.
(44) Chakravarthy, R.; Naik, G. N.; Savalia, A.; Sridharan, U.; Saravanan, C.; Das, A. K.; Gudasi, K. B. *Energy Fuels* **2016**, *30*, 8579−8586.
(45) Fan, T.-P. *Energy Fuels* **1991**, *5*, 371−375.
(46) Lobodin, V. V.; Robbins, W. K.; Lu, J.; Rodgers, R. P. *Energy Fuels* **2015**, *29*, 6177−6186.
(47) Hsu, C. S.; Qian, K.; Robbins, W. K. *J. High Resolut. Chromatogr.* **1994**, *17*, 271−276.
(48) Valencia-dávila, J. A.; Blanco-tirado, C.; Combariza, M. Y. *Fuel* **2017**, *193*, 168−177.
(49) Vasconcelos, G. A.; Pereira, R. C. L.; Santos, C. D. F.; Carvalho, V. V.; Tose, L. V.; Romão, W.; Vaz, B. G. *Int. J. Mass Spectrom.* **2017**, *418*, 67−72.
(50) Clingenpeel, A. C.; Rowland, S. M.; Corilo, Y. E.; Zito, P.; Rodgers, R. P. *Energy Fuels* **2017**, *31*, 5933−5939.
(51) Clingenpeel, A. C.; Robbins, W. K.; Corilo, Y. E.; Rodgers, R. P. *Energy Fuels* **2015**, *29*, 7150−7155.
(52) Jarvis, J. M.; Robbins, W. K.; Corilo, Y. E.; Rodgers, R. P. *Energy Fuels* **2015**, *29*, 7058−7064.
(53) Boduszynski, M. M.; Hurtubise, R. J.; Silver, H. F. *Anal. Chem.* **1982**, *54*, 375−381.
(54) Gutiérrez, L. B.; Ranaudo, M. a.; Méndez, B.; Acevedo, S. *Energy Fuels* **2001**, *15*, 624−628.
(55) Spiecker, P. M.; Gawrys, K. L.; Kilpatrick, P. K. *J. Colloid Interface Sci.* **2003**, *267*, 178−193.
(56) Wattana, P.; Fogler, H. S.; Yen, A.; Del Carmen García, M.; Carbognani, L. *Energy Fuels* **2005**, *19*, 101−110.
(57) Acevedo, S.; Castro, A.; Vásquez, E.; Marcano, F.; Ranaudo, M. A. *Energy Fuels* **2010**, *24*, 5921−5933.
(58) Boysen, R. B.; Schabron, J. F. *Energy Fuels* **2013**, *27*, 4654−4661.
(59) Buenrostro-Gonzalez, E.; Andersen, S. I.; Garcia-Martinez, J. A.; Lira-Galeana, C. *Energy Fuels* **2002**, *16*, 732−741.
(60) Rogel, E.; Ovalles, C.; Moir, M. *Energy Fuels* **2012**, *26*, 2655−2662.
(61) Acevedo, S.; Escobar, O.; Echevarria, L.; Gutiérrez, L. B.; Méndez, B. *Energy Fuels* **2004**, *18*, 305−311.
(62) Subramanian, S.; Simon, S.; Gao, B.; Sjoblom, J. *Colloids Surf., A* **2016**, *495*, 136−148.
(63) Subramanian, S.; Sorland, G. H.; Simon, S.; Xu, Z.; Sjoblom, J. *Colloids Surf., A* **2017**, *514*, 79−90.
(64) Nascimento, P. T. H.; Santos, A. F.; Yamamoto, C. I.; Tose, L. V.; Barros, E. V.; Gonçalves, G. R.; Freitas, J. C. C.; Vaz, B. G.; Romão, W.; Scheer, A. P. *Energy Fuels* **2016**, *30*, 5439−5448.
(65) Hurt, M. R.; Borton, D. J.; Choi, H. J.; Kenttämaa, H. I. *Energy Fuels* **2013**, *27*, 3653−3658.
(66) Jarrell, T. M.; Jin, C.; Riedeman, J. S.; Owen, B. C.; Tan, X.; Scherer, A.; Tykwinski, R. R.; Gray, M. R.; Slater, P.; Kenttämaa, H. I. *Fuel* **2014**, *133*, 106−114.
(67) Borton, D.; Pinkston, D. S.; Hurt, M. R.; Tan, X.; Azyat, K.; Scherer, A.; Tykwinski, R.; Gray, M.; Qian, K.; Kenttämaa, H. I. *Energy Fuels* **2010**, *24*, 5548−5559.
(68) Chacón-Patiño, M. L.; Vesga-Martínez, S. J.; Blanco-Tirado, C.; Orrego-Ruiz, J. A.; Gómez-Escudero, A.; Combariza, M. Y. *Energy Fuels* **2016**, *30*, 4550−4561.
(69) Kaiser, N. K.; Quinn, J. P.; Blakney, G. T.; Hendrickson, C. L.; Marshall, A. G. *J. Am. Soc. Mass Spectrom.* **2011**, *22*, 1343−1351.
(70) Blakney, G. T.; Hendrickson, C. L.; Marshall, A. G. *Int. J. Mass Spectrom.* **2011**, *306*, 246−252.
(71) Corilo, Y. E. *PetroOrg Software*; Florida State University: Tallahassee, FL, 2017; http://www.petroorg.com.
(72) Gawrys, K. L.; Blankenship, G.; Kilpatrick, P. K. *Energy Fuels* **2006**, *20*, 705−714.
(73) Klein, G.; Kim, S.; Rodgers, R.; Marshall, A. G.; Yen, A. *Energy Fuels* **2006**, *20*, 1973−1979.
(74) McKenna, A. M.; Purcell, J. M.; Rodgers, R. P.; Marshall, A. G. *Energy Fuels* **2009**, *23*, 2122−2128.
(75) Ali, M. F.; Perzanowski, H.; Bukhari, A.; Al-Haji, A. A. *Energy Fuels* **1993**, *7*, 179−184.
(76) Smith, D. F.; Rahimi, P.; Teclemariam, A.; Rodgers, R. P.; Marshall, A. G. *Energy Fuels* **2008**, *22*, 3118−3125.
(77) Chacón-Patiño, M. L.; Blanco-Tirado, C.; Orrego-Ruiz, J. A.; Gómez-Escudero, A.; Combariza, M. Y. *Energy Fuels* **2015**, *29*, 6330−6341.
(78) Klein, G.; Kim, S.; Rodgers, R.; Marshall, A.; Yen, A.; Asomaning, S. *Energy Fuels* **2006**, *20*, 1965−1972.
(79) Rogel, E.; Witt, M. *Energy Fuels* **2017**, *31*, 3409−3416.

DOI: 10.1021/acs.energyfuels.7b03281
Energy Fuels 2018, 32, 314−328

(80) Parida, S. K.; Dash, S.; Patel, S.; Mishra, B. K. *Adv. Colloid Interface Sci.* **2006**, *121*, 77−110.
(81) Leyden, D. E. *Silanes, Surfaces, and Interfaces*; Gordon and Breach: New York, 1986.
(82) Chacón-Patiño, M. L.; Blanco-Tirado, C.; Orrego-Ruiz, J. A.; Gómez-Escudero, A.; Combariza, M. Y. *Energy Fuels* **2015**, *29*, 1323−1331.
(83) Nassar, N. N.; Hassan, A.; Pereira-Almao, P. *Energy Fuels* **2011**, *25*, 1017−1023.
(84) Nassar, N. N.; Hassan, A.; Pereira-almao, P. *J. Colloid Interface Sci.* **2011**, *360*, 233−238.
(85) Franco, C.; Montoya, T.; Nassar, N. N.; Pereira-almao, P.; Cortes, F. B. *Energy Fuels* **2013**, *27*, 7336−7347.
(86) Buenrostro-Gonzalez, E.; Groenzin, H.; Lira-Galeana, C.; Mullins, O. C. *Energy Fuels* **2001**, *15*, 972−978.
(87) Groenzin, H.; Mullins, O. C.; Eser, S.; Mathews, J.; Yang, M.-G.; Jones, D. *Energy Fuels* **2003**, *17*, 498−503.
(88) Jonker, M. T. O.; Koelmans, A. A. *Environ. Sci. Technol.* **2002**, *36*, 4107−4113.
(89) Barnabas, I. J.; Dean, J. R.; Fowlis, I. A.; Owen, S. P. *Analyst* **1995**, *120*, 1897−1904.
(90) Giraldo-Dávila, D.; Chacón-Patiño, M. L.; Orrego-Ruiz, J. A.; Blanco-Tirado, C.; Combariza, M. Y. *Fuel* **2016**, *185*, 45−58.
(91) Marquez, N.; Ysambertt, F.; De La Cruz, C. *Anal. Chim. Acta* **1999**, *395*, 343−349.
(92) Bisht, H.; Reddy, M.; Malvanker, M.; Patil, R. C.; Gupta, A.; Hazarika, B.; Das, A. K. *Energy Fuels* **2013**, *27*, 3006−3013.
(93) Speight, J. G.; Long, R. B. *Fuel Sci. Technol. Int.* **1996**, *14*, 1−12.
(94) Strausz, O. P.; Torres, M.; Lown, E. M.; Safarik, I.; Murgich, J. *Energy Fuels* **2006**, *20*, 2013−2021.
(95) Juyal, P.; McKenna, A. M.; Fan, T.; Cao, T.; Rueda-Velásquez, R. I.; Fitzsimmons, J. E.; Yen, A.; Rodgers, R. P.; Wang, J.; Buckley, J. S.; Gray, M. R.; Allenson, S. J.; Creek, J. *Energy Fuels* **2013**, *27*, 1899−1908.
(96) Loegel, T. N.; Danielson, N. D.; Borton, D. J.; Hurt, M. R.; Kenttämaa, H. I. *Energy Fuels* **2012**, *26*, 2850−2857.
(97) Tapio, L.; Subramanian, S.; Simon, S.; Sjöblom, J. *J. Dispersion Sci. Technol.* **2017**, *38*, 355−360.
(98) Rogel, E.; Witt, M. *Energy Fuels* **2016**, *30*, 915−923.
(99) Adams, J. J. *Energy Fuels* **2014**, *28*, 2831−2856.
(100) Wang, S.; Liu, Q.; Tan, X.; Xu, C.; Gray, M. *Energy Fuels* **2013**, *27*, 2465−2473.
(101) Marczewski, A.; Szymula, M. *Colloids Surf., A* **2002**, *208*, 259−266.
(102) Subramanian, S.; Simon, S.; Gao, B.; Sjoblom, J. *Colloids Surf., A* **2016**, *495*, 136−148.

DOI: 10.1021/acs.energyfuels.7b03281
Energy Fuels 2018, 32, 314−328